

Transverse and secondary voltages in $\text{Bi}_2\text{Sr}_2\text{CaCu}_2\text{O}_8$ single crystals

K. Vad¹, S. Mészáros¹, and B. Sas²

Institute of Nuclear Research, P.O.Box 51, H-4001 Debrecen, Hungary

² *Research Institute of Solid State Physics, P.O.Box 49, H-1525 Budapest, Hungary*

(Dated: June 22, 2018)

Multicontact configuration is one of the most powerful arrangements for electrical transport measurements applied to study vortex phase transition and vortex phase dimensionality in strongly anisotropic high- T_c superconducting materials. In this paper we present electrical transport measurements using a multiterminal configuration, which prove both the existence of guided vortex motion in $\text{Bi}_2\text{Sr}_2\text{CaCu}_2\text{O}_8$ single crystals near the transition temperature and that secondary voltage in zero external magnetic field is induced by thermally activated vortex loop unbinding. The phase transition between the bound and unbound states of the vortex loops was found to be below the temperature where the phase coherence of the superconducting order parameter extends over the whole volume of the sample. We show experimentally that 3D/2D phase transition in vortex dimensionality is a length-scale-dependent layer decoupling process and takes place simultaneously with the 3D/2D phase transition in superconductivity at the same temperature.

I. INTRODUCTION

In the mixed state of isotropic type II superconductors the vortices can move in the direction of the Lorentz force due to transport currents. The angle between the local transport current density and the direction of the electric field induced by vortex motion is the Hall angle, which can be determined experimentally by measuring the Hall voltage. If the superconducting system has structural inhomogeneities, the direction of vortex velocity can differ from that of the Lorentz force. This misalignment between the directions of vortex velocity and the Lorentz force can be identified by observing an even transverse voltage, which, as opposed to the odd Hall voltage, does not change sign upon magnetic field reversal. This transverse voltage can be attributed to guided vortex motion, where vortices move along in a particular direction determined by the structure of the sample.

Guided vortex motion has been observed in classical type II superconductors¹ and is expected to be more pronounced in high- T_c materials. In $\text{YBa}_2\text{Cu}_3\text{O}_{7-\delta}$ single crystals it can be induced by twin boundaries, as it has been proved by magneto-optical technique², magnetization³ and transverse voltage⁴ measurements. These results confirm that vortices move in a channel, formed at one edge of a twin boundary along the twin planes. The other possibility of guided vortex motion is the intrinsic channelling between CuO_2 planes due to intrinsic pinning. This effect in La-Sr-Cu-O superconductors was observed by C.A. Durán *et al.*⁵ and in $\text{YBa}_2\text{Cu}_3\text{O}_{7-\delta}$ films by P. Berghuis *et al.*⁶. Channel formation in 2H-NbSe₂ at relatively low temperatures was experimentally studied by Z. Xiao *et al.*⁷. It was shown that depinning of a strongly pinned vortex lattice starts through the formation of weakly pinned regions in which the vortices start moving first. In $\text{Bi}_2\text{Sr}_2\text{CaCu}_2\text{O}_x$ guided vortex motion was studied

by the Hall resistivity measurements in textured samples⁸. To our knowledge, in $\text{Bi}_2\text{Sr}_2\text{CaCu}_2\text{O}_8$ single crystals the existence of guided vortex motion has not been proven yet.

Of high- T_c superconducting compounds $\text{Bi}_2\text{Sr}_2\text{CaCu}_2\text{O}_8$ is preferred because, due to its extremely high anisotropy, its discrete superconducting layers play an important role in current conduction properties even in the transition temperature range, and, due to the highly anisotropic conductivity, the vortex matter has a very rich phase diagram with numerous phase transitions. The multicontact configuration is one of the most promising arrangements of electrical transport measurements in the study of superconducting phase transition and vortex dimensionality. In this configuration four electrical contacts are attached to one side of a single crystal and two or four contacts to the opposite side. If the current injected into one side of a crystal is high enough, a voltage drop on both sides can be measured. The side where the current is injected is called primary, the opposite side is secondary. Due to this contact arrangement and the anisotropic conductivity, a non-uniform current distribution develops in the sample, and the current injected into the primary side is confined to a very thin surface layer, which is thinner than the thickness of the crystal. If the pancakes in adjacent layers belonging to the same vortex line are strongly coupled to each other, the primary current induces vortex motion not only in the primary, but also in the secondary surface, causing non-local dissipation in the sample. Moreover, if the coupling strength between the pancakes is high enough to produce three-dimensional (3D) type vortex lines across the sample, primary and secondary voltages can be equal. This configuration reminds us of the geometry used by I. Giaever in his famous experiment⁹, which is called dc flux transformer configuration.

The first measurements on $\text{Bi}_2\text{Sr}_2\text{CaCu}_2\text{O}_8$ single crystals using the dc flux transformer configuration were performed by H. Safar *et al.*¹⁰ and R. Busch *et al.*¹¹. They observed the dimensionality of the vortex system over a wide range of the phase diagram. Y.M. Wan *et al.*^{12,13} and C.D. Keener *et al.*¹⁴ also used the multicontact dc flux transformer configuration to study the secondary voltage and found that in magnetic fields near the transition temperature the interlayer vortex coupling was responsible for the secondary voltage. However, the origin of the secondary voltage in zero external magnetic field still remained problematic. S.W. Pierson¹⁵ suggested that it originated from thermally activated vortex loop unbinding. A vortex loop is a correlated vortex-antivortex line pair. Using a real-space renormalization group analysis, the author identified three characteristic critical currents and calculated their temperature dependence. He found that the temperature dependence of the secondary voltage is a horizontal slice of the current-temperature phase diagram.

In this paper we present electrical transport measurements using a multiterminal configuration that prove the existence of guided vortex motion in chemically and mechanically homogeneous $\text{Bi}_2\text{Sr}_2\text{CaCu}_2\text{O}_8$ single crystals. We also present the implications of experimental results for the 3D/2D phase transition in vortex dimensionality near the Ginzburg-Landau transition temperature and show that this phase transition is a length-scale-dependent layer decoupling process. We show that the temperature dependence of the secondary voltage in zero magnetic field has a double peak structure.

II. EXPERIMENTAL ARRANGEMENT

Single-crystalline $\text{Bi}_2\text{Sr}_2\text{CaCu}_2\text{O}_8$ compounds were prepared by the melt cooling technique, described in Reference¹⁶. Optically smooth rectangular crystals were carefully cleaved from these compounds, and heated in flowing oxygen for 15 minutes at 900 K in order to stabilize the oxygen content. Chemical homogeneity of the samples was checked by microbeam PIXE and (O^{16}, α) resonant elastic scattering¹⁷ with a spatial resolution of 5 μm . No chemical inhomogeneities were identified. The surface smoothness was measured by atomic force microscopy. The surfaces were found to be flat with a typical roughness of 10 nm. Before preparing the electrical contacts, the sample quality was checked by magnetization measurements using a SQUID or a vibrating sample magnetometer, and by AC susceptibility measurements. Electrical contacts were made by bonding 25 μm gold wires with Dupont 6838 silver epoxy fired for five minutes

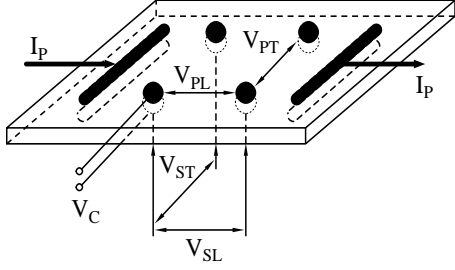


FIG. 1: Electrode configuration used for transverse and secondary voltage measurements. For definition of voltages see text. I_P denotes the primary current.

at 900 K. The contact resistance was a few ohms. The geometrical position of electrical contacts was precisely measured by optical microscope.

Two current and four potential electrodes were attached to both faces of the crystals. The scheme of the electrode configuration is shown in Fig. 1. The current was injected into one face of the single crystal through the current contacts (this is the primary current I_P), while primary and secondary longitudinal voltages, primary and secondary transverse voltages, and the voltage between the two faces were recorded simultaneously, using a six-channel data acquisition system. Applying this symmetrical contact arrangement, this configuration made it possible to check the sample homogeneity from the point of view of electrical conductivity.

We have performed measurements on a number of crystals, but in this paper we present the results we measured on two of them fabricated from the same batch (samples *A* and *B*). The mean-field Ginzburg-Landau (GL) transition temperatures T_{c0} of the samples were 88.5 K and 88 K, respectively. The sample dimensions were about $1 \times 1.5 \text{ mm}^2$, the thickness was 8 and 3 μm , respectively. As we pointed out in our previous papers¹⁸, most of the Joule heat due to the transport current was generated in the current contacts. In order to reduce the heat dissipation, and also to eliminate the thermoelectric force, we used current pulses with a duration time of 1 ms and repetition time of 100 ms. This arrangement and the fact that the sample temperature was regulated by a temperature controlled He gas stream instead of exchange gas, made it possible to avoid heating during the pulse up to the amplitude of 10 mA.

In our experiments the following voltages, shown in Fig. 1, were simultaneously recorded: (i) longitudinal voltages measured parallel to the current direction on the surface of the crystal where the current was injected and on the opposite surface (V_{PL} and V_{SL} , the primary and secondary longitudinal voltages, respectively); (ii) the primary and secondary transverse voltages, measured perpendicularly to the current direction (V_{PT} and V_{ST}); (iii) the *c*-axis di-

reaction voltage measured between the two surfaces of the crystal (V_C).

Using the analysis of R. Busch *et al.*¹¹, we could define the temperature dependence of the ab plane and c -axis resistivities from the voltages V_{PL} and V_{SL} . For the anisotropy ratio γ we received $\gamma = \sqrt{(\rho_c/\rho_{ab})} \approx 500$ with $\rho_{ab} \approx 100 \mu\Omega\text{cm}$ at 90 K.

III. EXPERIMENTAL RESULTS

The temperature dependence of the primary longitudinal and transverse voltages, V_{PL} and V_{PT} , of a $\text{Bi}_2\text{Sr}_2\text{CaCu}_2\text{O}_8$ single crystal (sample *A*) measured in zero and 1 T magnetic fields is shown in Fig. 2(a and b). In zero magnetic field V_{PT} shows a sharp change in the transition temperature range with a sign reversal. This sign reversal also exists in weak magnetic fields and seems to be a universal characteristic of vortex motion. Fig. 2(c) shows the calculated ratio of the measured primary transverse and longitudinal voltages in zero and 1 T magnetic fields. The maximum value of this ratio in zero magnetic field is 6, and it is larger than 1 in a temperature range of ~ 3 K. In 1 T magnetic field the maximum value is only 1.5 and the temperature range where the ratio is larger than 1 is 14 K wide. The Hall voltage can be calculated from the difference of the two transverse voltages measured in a magnetic field (here 1 T) with opposite field directions (Fig. 2(b)).

On the secondary side of the crystal we found that in zero magnetic field the ratio of transverse and longitudinal voltages, V_{ST} and V_{SL} , is higher than 1 in a temperature range of ~ 0.7 K (Fig. 3). This range is about 4 times narrower than it is on the primary side. In higher magnetic fields, with the field perpendicular to the ab plane, we could not determine this ratio because both V_{ST} and V_{SL} decreased to lower than 100 nV at 5 mA measuring current already in 100 mT magnetic field. Sample *B*, prepared to study the parallel case, was placed in the cryostat so that the ab planes were parallel to the magnetic field direction. In this arrangement V_{SL} is detectable in high magnetic fields. The result is presented in Fig. 4.

In zero applied magnetic field the secondary voltage is determined by interlayer vortex coupling. In order to gain information about this coupling strength, we measured the voltage V_C between the two surfaces of the crystal while applying a primary current I_P . Depending on the current distribution in the crystal, some part of this current flows in the c -axis direction and V_C depends on this current. The temperature dependence of V_C is of metallic ($d\rho/dT > 0$) type, except in a small temperature range near the mean-field Ginzburg-Landau transition temperature. In Fig. 5(a) this range is between

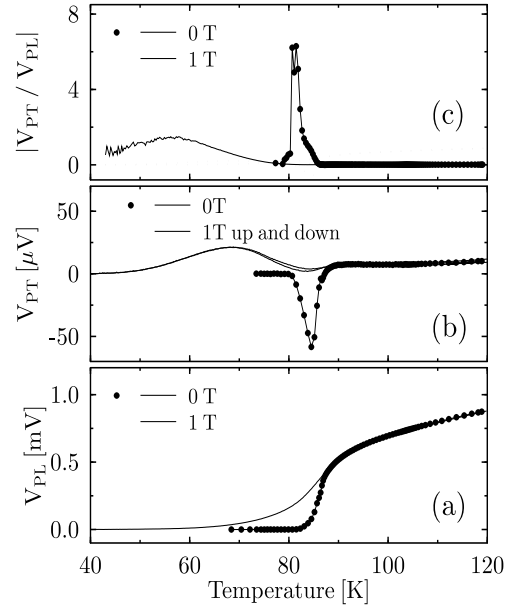


FIG. 2: Temperature dependence of the primary longitudinal voltage V_{PL} (a), primary transverse voltage V_{PT} (b) and the absolute value of the V_{PT}/V_{PL} ratio (c) of a $\text{Bi}_2\text{Sr}_2\text{CaCu}_2\text{O}_8$ single crystal measured in zero and 1 T magnetic fields. In (b) V_{PT} is measured in two opposite magnetic field directions. The magnetic field is perpendicular to the ab planes, $I_P = 1$ mA.

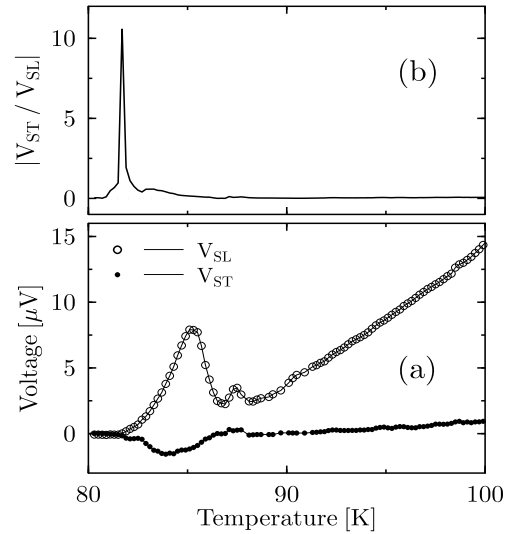


FIG. 3: Temperature dependence of the secondary longitudinal V_{SL} and transverse V_{ST} voltages (a) and the absolute value of the V_{ST}/V_{SL} ratio (b), $I_P = 1$ mA.

85 and 86 K. This temperature dependence is also reflected in the current-voltage characteristics (Fig. 5(b)). Far above the GL transition temperature, at 256 K the current-voltage characteristic is linear. Near the GL transition temperature, at 87.3 K there is a slight curvature in it. On further cooling the sample from 87.3 K to 86 K the curvature increases.

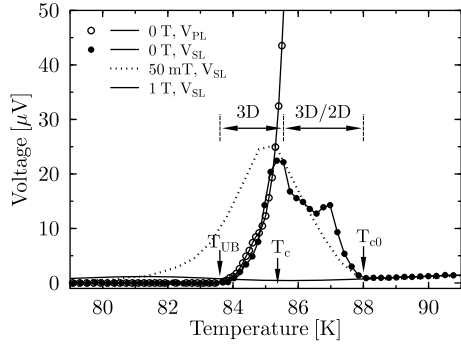


FIG. 4: Secondary and primary voltages vs. temperature in different magnetic fields (sample *B*). The magnetic field is parallel to the *ab* planes, $I_P = 1$ mA. T_{UB} , T_c and T_{c0} denote the unbinding, transition and Ginzburg-Landau transition temperature, respectively. The different vortex dimensionalities are also shown.

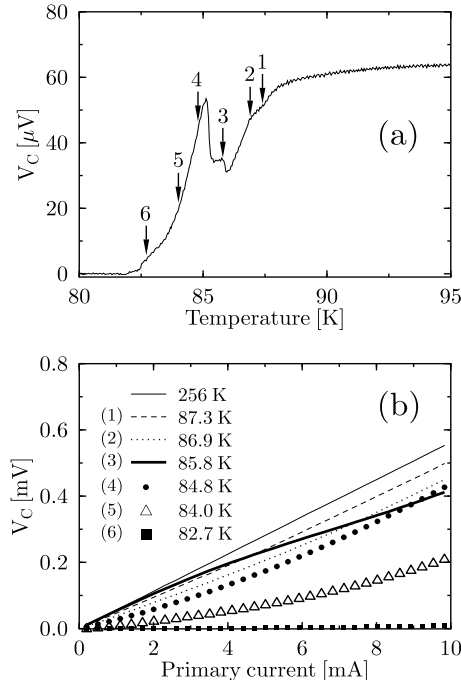


FIG. 5: Temperature dependence of V_C at 1 mA primary current (a), and current-voltage characteristics measured at different temperatures (b) in zero magnetic field. The arrows in (a) denote the temperatures where the current-voltage characteristics were measured.

In the temperature range between 86 K and 85 K the $I_P - V_C$ curves are concave in shape (for clarity in Fig. 5 we present only the curve measured at 85.8 K). At temperatures lower than 85 K both the $V_C - I_P$ and $V_C - T$ curves show the same metallic behaviour, as above 86 K.

IV. DISCUSSION

A. Guided vortex motion

The experimental results discussed above can help us to understand the origin of transverse voltages. In general, transverse voltage consists of three components: a component coming from the geometrical misalignment of the contacts, a Hall voltage component, and a component originating from the guided motion of vortices. The geometrical misalignment can be detected by normal-state measurements. The other two components can be distinguished by comparing the voltages measured in two opposite magnetic field directions: while in the Hall voltage the sign of the measured voltage depends on the external magnetic field direction because the vortex motion is only governed by the Lorentz force, in the case of the guided vortex motion it is independent of the field direction. This difference gives us the chance to distinguish between these two voltage generation mechanisms. On the basis of our results we can conclude that the guided motion of vortices is reflected in both V_{PT} and V_{ST} transverse voltages (Fig. 2 and 3), and that in our samples the guided vortex motion is a dominating effect in the Hall voltage measurements, since the Hall voltage is superimposed on a voltage, which is found to be much higher than the Hall voltage itself (Fig. 2(b)).

In our electrode configuration the main part of the injected current I_P flows in the *ab* planes, but has a component in the *c*-axis direction, too. If the external magnetic field is parallel to the *c*-axis, the latter component of the current is parallel to the vortex lines, so, it does not contribute to the Lorentz force. The dominating component of the transverse voltage is brought about by the intralayer current.

There is a well-defined temperature range, where the ratio of transverse and longitudinal voltages is larger than 1, while the geometrical misalignment between the transverse voltage contacts is less than 10 % of the distance between the longitudinal voltage contacts, as it was measured by an optical microscope. This supports the view that the transverse voltage cannot originate from a geometrical misalignment of the potential contacts. Chemical inhomogeneity does not explain this phenomenon, either. We believe that these results can be understood within the concept of guided vortex motion. If the magnetic field is perpendicular to the *ab* planes, slight inhomogeneities in pinning potentials can bring about channels for moving vortices, which results in guided motion. Some vortices are localized by stronger pinning centers and form trapped vortex regions, other mobile vortices flow in channels between these trapped regions. The existence of such vortex channels decreases the critical current because the effective pinning potential is lower, con-

sequently, vortex mobility is higher in a channel than outside. Guided vortex motion is sensitive to applied magnetic fields. Higher magnetic fields restricts the guided motion of vortices through vortex-vortex interaction.

B. Secondary longitudinal voltage

In 2D superconducting layers the phase fluctuation of the order parameter generates vortex-antivortex pairs as topological excitations¹⁹. The phase transition in an isolated 2D superconducting layer, where the vortex-antivortex pairs are bound below the phase transition temperature and are unbound above it, is described by the Kosterlitz-Thouless theory^{20,21}. In thin films, if the film thickness is less than the superconducting coherence length, this Kosterlitz-Thouless phase transition (T_{KT}) can be observed.

In high-temperature superconductors, the high transition temperature, short coherence length and layered structure make the phase fluctuation of the order parameter dominant over the other fluctuations in the transition temperature range, but the coupling between superconducting layers modifies the 2D Kosterlitz-Thouless picture. The interaction between superconducting layers leads to vortex-antivortex interaction different from the 2D case. In $\text{Bi}_2\text{Sr}_2\text{CaCu}_2\text{O}_8$ single crystals the CuO_2 planes serve as 2D superconductor layers, the vortices are the pancake vortices. Due to the layered structure a high anisotropy exists in conductivity and the vortex matter has a very rich phase diagram with numerous phase transitions. Among others the 3D phase appears, where the coupling between neighbouring layers arranges the thermally excited pancake vortices into 3D flux lines²². These 3D flux lines can form vortex loops as correlated vortex-antivortex line pairs. They are called thermally activated vortex loops, because they are the result of a combined effect of thermally activated vortex excitation and interlayer vortex coupling.

The 3D character modifies the structure of the phase transition between the bound and unbound states. Although the 2D signatures are prevalent, a narrow 3D window appears around the phase transition temperature (T_c) and a nonzero critical current appears. The 3D temperature region is theoretically predicted and it has been shown that the size of this 3D region is much smaller above T_c than below²³. Above the phase transition temperature the behaviour of vortices becomes 2D due to decoupling of the superconducting layers (3D/2D phase transition). It has been also shown in another paper²⁴ that this layer decoupling is a length-scale-dependent process: the layers become decoupled at length scales larger than an interlayer screen-

ing length, while for lengths below this scale they remain coupled. The manifestation of the 3D/2D transition in electrical transport properties has not been investigated before.

In an isolated 2D superconducting layer the vortex pair energy is the sum of the creation energy of the two vortices and the intralayer logarithmic coupling energy between vortices. In layered systems like $\text{Bi}_2\text{Sr}_2\text{CaCu}_2\text{O}_8$ this vortex pair energy is modified by the interlayer Josephson coupling, which not only strengthens the intralayer interaction, but causes an interaction between vortices located in neighbouring layers. The intralayer vortex pair energy can be written in the following simple form: $E(r) = 2E_c + K_{\parallel} \ln(r/\xi_0) + K_{\perp} r/\xi_0$, where r is the distance between the vortex and antivortex, E_c is the creation energy of a vortex, ξ_0 is the zero-temperature correlation length, K_{\parallel} is the intralayer vortex-vortex coupling constant and K_{\perp} is the interlayer Josephson coupling constant. While the 2D logarithmic interaction (second term in this equation) dominates at short distances, the Josephson-coupling mediated 3D linear interaction (third term) dominates at large distances. The intralayer vortex length scale $R_{\lambda}(T)$ is the characteristic length which divides this logarithmic and linear regimes²⁴. $R_{\lambda}(T) = \xi_0/\sqrt{\lambda}$, where λ is the ratio of the interlayer Josephson coupling to the intralayer coupling, $\lambda = K_{\perp}/K_{\parallel}$. λ depends on the size r of the vortex pairs, and above T_c it has a maximum. The size r which belongs to this maximum λ is the other characteristic length, the interlayer screening length $l_{3D/2D}(T)$. If the separation between two vortices located in neighbouring layers is larger than $l_{3D/2D}$, the Josephson-coupling mediated linear interaction is screened out and the layers are decoupled. Around T_c the dimensional behaviour of the system is determined by these two characteristic lengths. The layers are coupled and the behaviour of vortices is 3D if the separation between vortices is greater than the intralayer vortex length scale $r > R_{\lambda}(T)$ and less than the interlayer screening length $r < l_{3D/2D}(T)$. The temperature dependence of $R_{\lambda}(T)$ and $l_{3D/2D}(T)$ shows²⁵ that the intralayer vortex length scale $R_{\lambda}(T)$ is constant for $T \ll T_c$, but it increases as the temperature approaches T_c from below. The interlayer screening length $l_{3D/2D}(T)$ decreases continuously as the temperature increases.

While in the 3D regime below T_c the electrical transport behaviour is dominated by vortex loops, above T_c it is dominated by vortex lines and pancake vortices. The multiterminal configuration is a good arrangement to distinguish between these two regimes. In this paper we show that studying the temperature dependence of the secondary voltage can help us to understand the length-scale-dependent layer decoupling, i.e., the 3D/2D phase

transition.

The secondary voltage has already been studied both theoretically¹⁵ and experimentally¹². It can now be accepted that in zero applied magnetic field it originates from thermally activated vortex loop unbinding. At low temperatures where V_{SL} and V_{PL} are zero, the thermally excited 3D flux lines form vortex loops which are 'pinned' to the crystal. With increasing temperature, the transport current splits these vortex loops into free vortex-antivortex line pairs. The temperature where this splitting starts is the unbinding temperature (T_{UB}). This is the lowest temperature where both V_{SL} and V_{PL} are observable. Above the unbinding temperature the free vortices move in the sample like 3D vortex lines due to the Lorentz force, producing the same voltage drop on the primary and secondary side of the crystal, $V_{PL} = V_{SL}$. This 3D character of the vortex lines remains up to a temperature where the secondary voltage has a local maximum. At sample *B* the 3D temperature range is around 85 K where the zero field primary and secondary longitudinal voltages $V_{PL}(0T)$ and $V_{SL}(0T)$ coincide (see Fig. 4). This is the same 3D temperature range which was predicted theoretically by renormalization group analysis²³. With increasing temperature the 3D character of flux motion disappears and consequently V_{SL} becomes lower than V_{PL} , but another local maximum of V_{SL} can be found as the temperature approaches T_{c0} . The temperature dependence of the secondary voltage has two peaks with a higher and a lower amplitude.

This double peak structure of $V_{SL}(0T)$ can be explained by the motion of different types of vortex lines. In zero applied magnetic field free vortex lines can be produced in two ways. First, they can be the result of vortex-antivortex depairing of thermally activated vortex loops due to the Lorentz force of the transport current. In this case the number of free vortex lines depends on the transport current density and a non-Ohmic behaviour characterizes the system. Secondly, free vortex lines can be spontaneously created by thermal activation, mainly above T_c . The number of free vortex lines increases with increasing temperature and the system is characterized by an Ohmic behaviour.

The effect of current on vortex-antivortex depairing is twofold. On the one hand the current reduces the creation energy whereby increases the density of vortex pairs. On the other hand the current exerts a force (the Lorentz force) on vortex loops and can blow them out. The number of blowouts depends on the size r of the vortex pairs. If r is higher than the intralayer vortex length scale $R_\lambda(T)$, the Josephson-coupling mediated 3D linear interaction is energetically favoured over 2D intralayer logarithmic interaction and the energy of a vortex loop is smaller than the energy of a pair of independent vortex lines. Be-

low T_c in $\text{Bi}_2\text{Sr}_2\text{CaCu}_2\text{O}_8$ $R_\lambda(T) = \xi_0/\sqrt{\lambda} \approx 1\mu\text{m}$, where $\xi_0 \sim 3\text{nm}$ and $\lambda \sim 10^{-5}$. Consequently, if $r > 1\mu\text{m}$, creation of vortex loops is energetically favoured over free vortex-antivortex line pairs. This happens in the 3D temperature range where the dominant topological excitation is the vortex loop. With increasing temperature the number of blowouts and, so, the longitudinal secondary voltage increases. However, approaching the transition temperature the intralayer vortex length scale $R_\lambda(T)$ starts to increase, therefore the number of vortex pairs which can be blown out by the transport current decreases which results in the decrease of the secondary voltage. The temperature which belongs to the peak value of the secondary voltage is the transition temperature T_c . Although at this temperature the behaviour of vortices is still 3D type as it was shown theoretically²⁵, the secondary voltage is somewhat lower than the primary voltage (see Fig. 4). This means that the secondary voltage starts to decrease before layer decoupling. At higher temperatures the 3D character of flux motion disappears and V_{SL} becomes significantly lower than V_{PL} . Above the 3D temperature range another local maximum of V_{SL} can be found as the temperature approaches T_{c0} , because the temperature is high enough to produce free vortex lines by thermal activation. The number of free vortex lines and, so, the secondary voltage increases with increasing temperature. The system is characterized by a continuous 3D/2D transition due to continuous decrease of the interlayer screening length $l_{3D/2D}(T)$ as the temperature approaches the mean-field Ginzburg-Landau transition temperature T_{c0} . Near T_{c0} the amplitude of the order parameter decreases, just as the number of the free vortex lines. This effect evokes the decrease of the secondary voltage. The temperature which belongs to the minimum secondary voltage above the double peak structure is T_{c0} .

The local maxima of V_{SL} can be decreased by magnetic field. If the magnetic field is perpendicular to the *ab* planes, the external field prevents the free motion of vortex-antivortex line pairs. While one part of a pair, which is parallel to the external magnetic field, cannot move in the sample because of the vortex-vortex interaction, the other antiparallel part is annihilated in the external magnetic field. If the magnetic field is parallel to the *ab* planes, there is no interaction between the vortex lattices formed by the external magnetic field and vortex loops, and the secondary voltage is not so sensitive to the applied magnetic field. In this arrangement the magnetic field reduces the coupling strength between the CuO_2 bilayers by decreasing both the magnetic and Josephson coupling. This has a twofold consequence. First, the thermally excited 2D vortex-antivortex pair creation in CuO_2 bilayers is suppressed by magnetic field because the creation

of a vortex-antivortex pair is equivalent to the creation of a dislocation in the interlayer flux line lattice which increases the elastic energy of the lattice. Secondly, the magnetic field reduces the probability of arrangement of thermally excited pancake vortices into 3D flux lines. That is why only one peak exists in low magnetic fields (50 mT) instead of a double peak (Fig. 4).

Information about the strength of Josephson coupling and the 2D/3D phase transition in superconductivity can be obtained by study the temperature dependence of $I_P - V_C$. In the temperature range where the $I_P - V_C$ curves are concave (between 85 and 86 K) the superconducting coherent state exists in the CuO₂ bilayers, but the interlayer coupling is not strong enough to establish the *c*-axis coherence. In consequence, the current in *c*-axis direction is carried by single particle tunnelling instead of Cooper pair tunnelling (2D type superconductivity). With the decrease in temperature, at 85 K, the Josephson coupling, and consequently, a phase coherence between superconducting bilayers develops and extends over the whole volume of the sample, producing maximum values in both V_{SL} and V_C (2D/3D phase transition). At temperatures lower than 85 K the Josephson coupling energy increases, the phase coherence of the superconducting order parameter extends over the whole volume of the sample and develops the 3D type superconductivity. The higher peak value of V_{SL} is also at 85 K which is the upper end of the temperature range where vortex lines have 3D character. Consequently 2D/3D phase transition in superconductivity and in vortex dimensionality takes place at the same temperature. This can be valid inversely, too. If the vortex dimensionality decreases from 3D to 2D, the dimensionality of superconductivity can also decrease. This result was experimentally supported by transport current measurements²⁶, where the authors proved that the Bardeen-Stephen model for the flux flow resistance $\rho_f = \rho_n \cdot B/B_{c2}$ (ρ_n , B and B_{c2} are the normal state resistivity, magnetic field and critical magnetic field) is not valid at high current density in Bi₂Sr₂CaCu₂O₈ single crystals. Due to intensive flux motion both the phase coherence between superconducting bilayers and the interlayer screening length $l_{3D/2D}(T)$ decrease resulting in a 3D/2D phase transition in dimensionality of superconduc-

tivity.

Thermally unbound vortex-antivortex line pairs take part in guided motion. The maximum values of $|V_{PT}/V_{PL}|$ and $|V_{ST}/V_{SL}|$ are near the unbinding temperature in the 3D type superconducting regime. So, the guided vortex motion has a 3D character in Bi₂Sr₂CaCu₂O₈ single crystals and develops due to melting of vortex loop lattice. The external magnetic field which is perpendicular to the *ab* planes restricts the guided motion of vortices through vortex-vortex interaction. That is why weak magnetic fields can prevent the development of secondary transverse voltage.

V. CONCLUSIONS

In conclusions, we found that temperature dependence of secondary longitudinal voltage has a double-peak structure and its higher maximum value is at the temperature where the phase coherence of the order parameter extends over the whole sample. Secondary voltage originates from correlated vortex-antivortex line pair unbinding, i.e., from vortex loop unbinding due to the Lorentz force of the transport current. Near T_{c0} free vortex-antivortex line pairs are also generated by thermally activated vortex excitation. We think that the two types of vortex-antivortex line pairs are responsible for the double peak structure of the secondary longitudinal voltage. Lacking of theories describing the double peak structure in Bi₂Sr₂CaCu₂O₈ single crystals indicates a need for better description of length-scale dependence in layered superconductors. In order to improve the theoretical description, one can perform the renormalization group analysis of Reference²⁷ for non-constant current density or one can use different renormalization group methods, e.g., field theoretical renormalization group approaches²⁸.

VI. ACKNOWLEDGEMENT

We take great pleasure in acknowledging discussion with P.F. de Châtel and I. Nándori. This work was supported by the Hungarian Science Foundation (OTKA) under contract no. T037976.

¹ M. Danckwert, A.R. Goñ and C. Thomsen, Phys. Rev. B **59**, R6624 (1999).

² V.K. Vlasko-Vlasov, L.A. Dorosinskii, A.A. Polyaskii, V.I. Nikitenko, U. Welp, B.W. Veal and G.W. Crabtree, Phys. Rev. Lett. **72**, 3246 (1994).

³ M. Oussena, P.A.J. de Groot, S.J. Porter, R. Gagnon and L. Taillefer, Phys. Rev. B **51**, 1389 (1995).

⁴ V.V. Chabanenko, A.A. Prodan, V.A. Shklovskij, A.V. Bondarenko, M.A. Obolemskii, H. Szymczak and S. Piechota, Physica C **314**, 133 (1999).

⁵ C.A. Durán, P.L. Gammel and D.J. Bishop, J. Appl. Phys. **79**, 6592 (1996).

⁶ P. Berghuis, E. Di Bartolomeo, G.A. Wagner and J.E. Evetts, Phys. Rev. Lett. **79**, 2332 (1997).

⁷ Z. Xiao, L.E.Y. Andrei, P. Shuk and M. Greenblatt, Phys. Rev. Lett. **86**, 2431 (2001).

⁸ P. Vašek, I. Janeček and V. Plecháček, Physica C **247**, 381 (1995).

⁹ I. Giaever, Phys. Rev. Lett. **15**, 825 (1965).

¹⁰ H. Safar, E. Rodriguez, F. de la Cruz, P.L. Gammel, L.F. Schneemeyer and D.J. Bishop, Phys. Rev. B **46**, 14238 (1992).

¹¹ R. Busch, G. Ries, H. Werthner, G. Kreiselmeyer and G. Saemann-Ischenko, Phys. Rev. Lett. **69**, 522 (1992).

¹² Y.M. Wan, S.E. Hebboul, D.C. Harris and J.C. Garland, Phys. Rev. Lett. **71**, 157 (1993).

¹³ Y.M. Wan, S.E. Hebboul and J.C. Garland, Phys. Rev. Lett. **72**, 3867 (1994).

¹⁴ C.D. Keener, M.L. Trawick, S.M. Ammirata, S.E. Hebboul and J.C. Garland, Phys. Rev. B **55**, R708 (1997); Phys. Rev. Lett. **78**, 1118 (1997).

¹⁵ S.W. Pierson, Phys. Rev. Lett. **74**, 2359 (1995); Phys. Rev. B **55**, 14536 (1997).

¹⁶ B. Keszei, Gy. Szabó, J. Vandlik, L. Pogány, and G. Oszlányi, J. Less Common Metals **155**, 229 (1989); J.R. Cooper, L. Forró and B. Keszei, Nature **343**, 444 (1990).

¹⁷ I. Rajta, I. Borbély-Kiss, Gy. Mórik, L. Bartha, E. Koltyay and Á.Z. Kiss, Nucl. Inst. and Methods B **109**, 148 (1996); T. Szörényi, Zs. Geretovszky, L. Kelemen, J. Tóth and A. Simon, Vacuum **59**, 327 (1998).

¹⁸ B. Sas, F. Portier, K. Vad, B. Keszei, L.F. Kiss, N. Hegmann, I. Puha, S. Mészáros and F.I.B. Williams, Phys. Rev. B **61**, 9118 (2000); F. Portier, G. Kriza, B. Sas, L.F. Kiss, I. Pethes, K. Vad, B. Keszei, N. and F.I.B. Williams, Phys. Rev. B **66**, 140511(R) (2002).

¹⁹ M. Tinkham, Introduction to Superconductivity (McGraw-Hill, New York, 1996).

²⁰ J.M. Kosterlitz and D.J. Thouless, J. Phys. C **6**, 1181 (1973).

²¹ B.I. Halperin and D.R. Nelson, J. Low Temp. Phys. **36**, 599 (1979).

²² G. Blatter, M.V. Feigel'man, V.B. Geshkenbein, A.I. Larkin and V.M. Vinokur, Reviews of Modern Physics **66**, 1125 (1994).

²³ S.W. Pierson, Phys. Rev. B **51**, 6663 (1995).

²⁴ S.W. Pierson, Phys. Rev. Lett. **75**, 4674 (1995).

²⁵ S.W. Pierson, Phys. Rev. B **54**, 688 (1995).

²⁶ I. Pethes, B. Sas, G. Kriza, F. Portier, F.I.B. Williams, K. Vad and S. Mészáros, Synthetic Metals **120**, 1013 (2001).

²⁷ S.W. Pierson, O.T. Valls, and H. Bahlouli, Phys. Rev. B **45**, 13035 (1992).

²⁸ I. Nándori, U.D. Jentschura, K. Sailer and G. Soff, Phys. Rev. D **69**, 025004 (2004) and J. Phys. G **28**, 607 (2002); I. Nándori, J. Polonyi and K. Sailer, Phil. Mag. B **81**, 1655 (2001) and Phys. Rev. D **63**, 045022 (2001).